

Halogenated Veneers: Protein Cross-Linking and Halogenation in the Jaws of *Nereis*, a Marine Polychaete Worm

Henrik Birkedal,^{*[a, b]} Rashda K. Khan,^[a] Nelle Slack,^[c, d] Chris Broomell,^[e] Helga C. Lichtenegger,^[a, f] Frank Zok,^[c] Galen D. Stucky,^{*[a, c]} and J. Herbert Waite^{*[a, e]}

Mineralized tissues are produced by most living organisms for load and impact functions. In contrast, the jaws of the clam worm, *Nereis*, are hard without mineralization. However, they are peculiarly rich in halogens, which are associated with a variety of post-translationally modified amino acids, many of which are multiply halogenated by chlorine, bromine, and/or iodine. Several of these modified amino acids, namely dibromohistidine, bromiodohistidine, chloriodotyrosine, bromiodotyrosine, chlorodityrosine, chlorotriptyrosine, chlorobromotriptyrosine, and bromiodotriptyrosine, have not been previously reported. We

have found that the distributions of Cl, Br, and I differ: Cl is widespread whereas Br and I, although not colocalized, are concentrated in proximity to the external jaw surfaces. By using nanoindentation, we show that Br and I are unlikely to play a purely mechanical role, but that the local Zn and Cl concentrations and jaw microstructure are the prime determinants of local jaw hardness. Several of the post-translationally modified amino acids are akin to those found in various sclerotized structures of invertebrates, and we propose that they are part of a cross-linked protein casing.

Introduction

Vertebrates use calcium containing minerals for tissue fortification, most notably in bones and teeth.^[1] Invertebrates, in contrast, exhibit more versatility in their choice of hard tissue chemistry. Iron biominerals, for example, are exploited in chiton teeth (iron oxides)^[2,3] and gastropod sclerites (iron sulfide).^[4] Exotic deposits of the copper biomineral, atacamite, reinforce regions of high stress in the jaws of the bloodworm, *Glycera*.^[5,6] Significant levels of inorganic elements, such as zinc and halogens, are present in the jaws of the clam worm, *Nereis* (Figure 1). Zinc is concentrated at the jaw tip,^[7-10] but there do not appear to be any mineral deposits. Recently, we showed that the zinc concentration correlates with the local hardness and elastic modulus.^[10] We also found that the local zinc concentration correlates with that of chlorine, and that there is a His gradient that appears to follow that of zinc, though the

amino acid was mapped on a much larger length scale. Combining this information with Zn extended X-ray absorption fine structure (EXAFS) and X-ray absorption near edge structure (XANES) data, we suggested that zinc acts as a cross-linker of

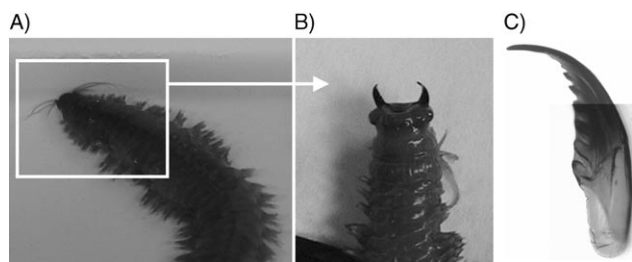


Figure 1. *N. virens* worm A) shown exploring, and B) with everted proboscis; the jaws are shown from the ventral side. C) A jaw extracted from the animal.

[a] Prof. Dr. H. Birkedal, R. K. Khan, Dr. H. C. Lichtenegger, Prof. Dr. G. D. Stucky, Prof. Dr. J. H. Waite
Department Chemistry and Biochemistry, University of California
Santa Barbara, CA 93106 (USA)
Fax: (+1) 805-893-4120
E-mail: stucky@chem.uscb.edu

[b] Prof. Dr. H. Birkedal
Department of Chemistry, University of Aarhus
140 Langelandsgade, 8000 Århus C (Denmark)
Fax: (+45) 861-96-199
E-mail: hbirkedal@chem.au.dk

[c] Dr. N. Slack, Prof. F. Zok, Prof. Dr. G. D. Stucky
Materials Department, University of California
Santa Barbara, CA 93106 (USA)

[d] Dr. N. Slack
Veeco Instruments, Inc., 112 Robin Hill Road, Santa Barbara, CA 93117 (USA)

[e] C. Broomell, Prof. Dr. J. H. Waite
Department of Molecular, Cellular, and Developmental Biology,
University of California, Santa Barbara, CA 93106 (USA)
E-mail: waite@lifesci.uscb.edu

[f] Dr. H. C. Lichtenegger
Present address: Institute of Materials Science and Technology
Vienna University of Technology,
9-11 Favoritenstraße, 1040 Vienna (Austria)

Supporting information for this article is available on the WWW under <http://www.chembiochem.org> or from the author: details of the mass spectrometric structure determination.

the proteinaceous matrix by forming $\text{Zn}(\text{His})_3\text{Cl}$ -like units.^[10] The larger hardness of the Zn-rich regions has also been shown with Vicker's hardness measurements by McClements et al.^[11] Thus, a key design feature appears to be the use of fine-tuned chemical gradients which adjust the local materials' properties. Gradients are a prominent feature of other invertebrate tissues, where they serve to moderate contact deformation between soft interior and harder exterior tissues,^[12] and have also emerged as a design principle for artificial materials.^[13]

Besides chlorine, *Nereis* jaws contain significant amounts of bromine and iodine.^[9,10] The aims of the present study were threefold: to determine a) the distribution of the halogens, b) whether the presence of halogens can be correlated with measurable mechanical properties in the jaw, and c) whether any halogens can be detected as organohalides. We report that these heavier halogens are concentrated near the outer surface of the jaw and appear, at least in part, to be present as halogenated amino acids, several of which are reported for the first time. The previously known amino acids are akin to those obtained from other sclerotized tissues and are suggestive of protein cross-linking.^[14–16]

Results and Discussion

Nereis jaws have a serrated and a smooth side, the former being used to grasp material when the two jaws are brought together in a bite (Figure 1).

We selected a transverse cut at the level of one of the dentitions, roughly 20% below the tip, for analysis. In both the optical and scanning electron microscopy (SEM) micrographs, sections of jaw interior revealed a texture that was spatially differentiated (Figure 2). The features described in the following were observed in several jaws.

First, channels of ~7 to ~20 μm in diameter (Figure 2A and inset) were found to extend through the length of the jaw.

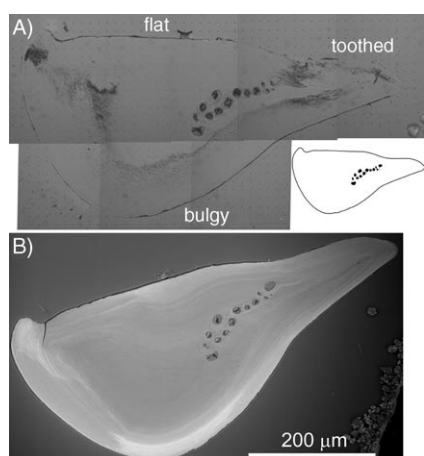


Figure 2. The transverse jaw cross-section under study. A) Composite optical micrograph after nanoindentation. Three characteristic regions are indicated. The inset illustrates the channels that run through the jaw. B) Back scattered electron micrograph. The contrast results from local variations in atomic number, Z ; see text for details.

These might be relics of the jaw growth process or access routes for cell-mediated repair of damaged jaws. *Nereis* jaws grow throughout the lifespan of the animal and jaw growth is associated with the formation of growth bands,^[17] but the details of jaw development and growth remain unknown. Second, areas of differential contrast were observed with both optical microscopy (Figure 2A) and SEM (Figure 2B). In the following we will refer to "smooth" and "dark" regions for the areas with low and high contrast, respectively. The exact origin of these different regions is unclear, but they could originate from variations in orientation of protein fibrils which lead to diverse local textures. Third, banding is observed on the back-scattered electron (BSE) images. The brightness in such images is proportional to the atomic number, Z ,^[18] and thus the large scattering intensity (equivalent to light features in Figure 2B) is indicative of a larger concentration of heavy elements. It is clear from the image in Figure 2B that there are regions that contain high- Z elements towards the rounded, outer surface of the jaw. We will henceforth refer to that side as the "bulgy side" while the opposing one will be named the "flat side" (Figure 2A).

The elemental distribution was analyzed by energy dispersive X-ray spectroscopy (EDS). In Figure 3, we show three such spectra taken at various points that move from the interior towards the exterior of the jaw, as indicated. The spectra show only signals from Zn, Cl, Br, I, and small amounts of Fe and Ca (O, C, N are, of course, also present in the sample, even though they are not shown in the spectra in Figure 3B–D). The I and Br signals are much stronger in the spectrum taken close to the sample surface (Figure 3D), while the Zn and Cl signals are slightly weaker near the sample surface than in the interior (Figure 3B). Using electron-microprobe analysis, we previously found that the Cl content is linearly related to the Zn concentration but with a nonzero offset,^[10] that is, even at zero Zn concentration, there is Cl in the jaw. Figure 3E shows a scan along the line marked in green in Figure 3A. The data are represented as $I/\langle I \rangle$, where I is the local intensity (corrected for background) and $\langle I \rangle$ is its average value. The scan clearly shows that Br and I are concentrated towards the sample exterior and that I localization coincides with the strong white bands in the BSE image (Figure 3A). This result is expected, since I has by far the largest atomic number of any of the elements detected in the jaw. However, I and Br are not colocalized: their distributions peak at opposite sides of the jaw.

The Zn and Cl signals, in contrast, are quite uniform over most of the jaw, but there is a step in the signals towards the flat side of the jaw which is indicative of a lower (Zn, Cl) concentration. Cl is found in higher relative abundance than Zn on one side of the jaw where the Br and I signals are strong; this suggests that perhaps the extra Cl is bound in a manner akin to that of Br and I (see chlorinated tyrosine derivatives in Table 1 and Scheme 1). These observations were confirmed by scans over the entire sample, which are shown in Figure 4. The Zn and Cl distributions are qualitatively parallel, and there are two regions with lower concentrations of Zn and Cl, as indicated in the Cl map. Br and I are concentrated in bands towards the jaw exterior; the Br band extends further into the jaw than

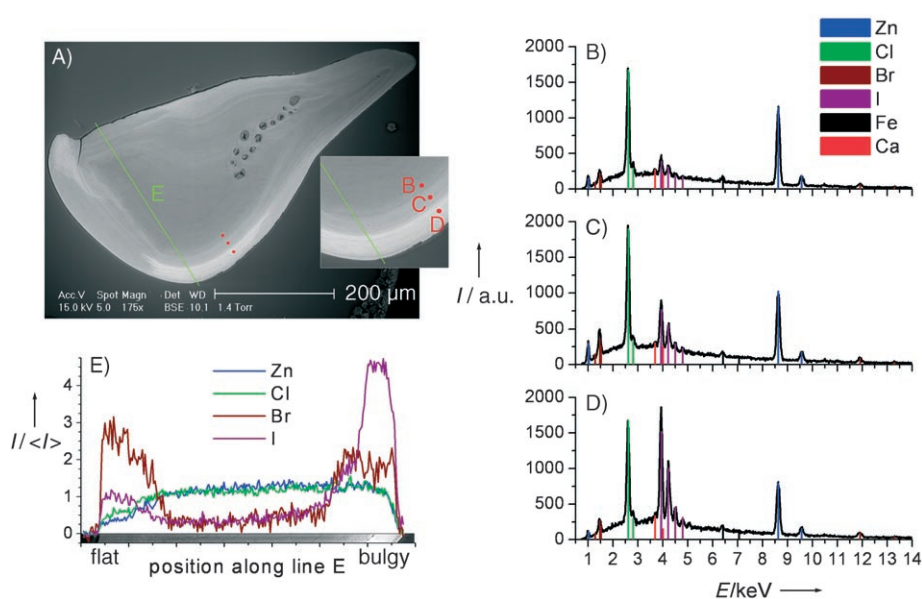


Figure 3. EDS X-ray analysis of the jaw cross-section. A) BSE image showing the points of interest investigated by using EDS. B)–D) EDS spectra measured at the points indicated in A) and inset, moving from the jaw interior (B) to the jaw exterior (D). Note the large increase in iodine concentration from B to D; units are energy (in keV) and intensity (in arbitrary units) of emitted X-rays for the ordinate and coordinate axes, respectively. E) EDS line scan carried out along the green trajectory shown in A). The X-ray intensities, I , were background corrected and normalized to the average intensity, $\langle I \rangle$, for each element. Thus a uniform distribution would give a value of 1 throughout. The inset below the curves shows the corresponding BSE image. Note that Zn and Cl are much more uniformly distributed than Br and I, which peak at the jaw edges.

Table 1. Substituents of amino acids isolated from *Nereis* jaw hydrolyzates. Amino acids not previously reported are marked by bold font. See Supporting Information for specific mass fragments used for identification and Scheme 1 for chemical structures of the side chains in question.

Amino acid	R ¹	R ²	Amino acid	R ¹	R ²
histidine	Br	Br	tyrosine	H	H
	Br	I		H	OH
	I	I		H	Cl
dityrosine	H	H	H	Br	
	H	Cl	Cl	Cl	
	H	Br	Cl	Br	
trityrosine	Br	Br	Cl	I	
	H	Cl	Br	Br	
	Cl	Br	Br	I	
	Br	I	I	I	

that of I. Note the similarity between the I map and the position of the white high-contrast band in the BSE image in Figure 3A.

Maps of local hardness (H) and modulus (\bar{E}) for the jaw cross section are presented in Figure 5. The mean values (from 610 indents) are $H=0.869$ and $\bar{E}=12.62$ GPa, with standard deviation and standard error of the mean of 0.161 and 0.007 GPa for H , and 1.76 and 0.07 GPa for \bar{E} . We stress that these values were obtained from dry samples and that hydration might yield different values for the mechanical properties. However, the local degree of hydration is unknown, which renders it difficult to experimentally correct for this problem. Measurements done on samples submerged in buffer show the same trends

as the data presented here.^[19]

The jaw cross-section can be largely divided into regions of lower- and higher-than-average hardness. The lower-than-average regions are outlined in Figure 5C. Two of these regions, marked I in this schematic representation, coincide with regions of lower Zn and Cl concentration identified in Figure 4. Thus, this explains, at least in part, the lower hardness of these regions since we previously found a linear correlation between hardness and Zn concentration.^[10] Throughout the rest of the jaw cross-section, the Zn concentration appears to be fairly constant, as can be seen in Figure 4 and, more clearly, in the line scans in Figure 3E. Hence, the lower hardness in the two regions labeled II must have a different origin. By comparing the position of the lower-than-average hard-

ness regions with the texture of the jaw cross-section seen in the micrograph in Figure 2A, we see that the softer regions coincide with regions of smooth texture in Figure 2A. This indicates that a prime determinant for hardness is the local mesostructure of the jaw. We speculate that variations in the orientation of the protein fibrils lead to the observed differences in indentation hardness.

As with the hardness, there are low-modulus regions in areas of lower Zn and Cl content, again this is in agreement with our previous observation of a correlation between both hardness, modulus, and Zn content.^[10] Besides this, regions of

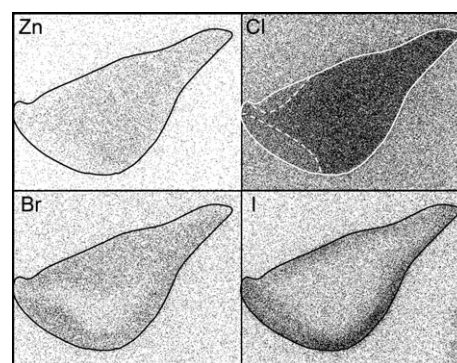


Figure 4. Element maps obtained by EDS display the concentrations of Br, I, Cl, and Zn throughout the jaw cross-section. The jaw outline is marked by a full black line except in the Cl map where it is in white. The dotted lines in the Cl map outline two regions of lower Zn and Cl concentration; see also Figure 3E. Br and I were found to be concentrated in bands near the jaw exterior.

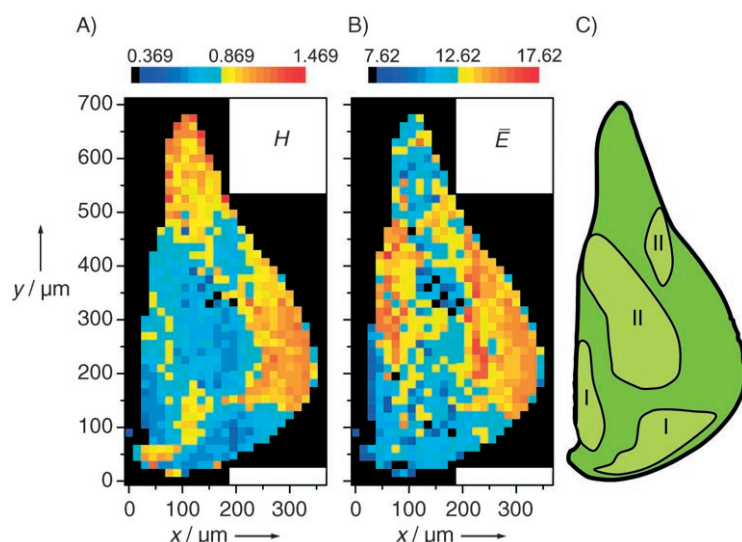


Figure 5. Local mechanical properties determined by nanoindentation on the transverse cross-section shown in Figure 2 and Figure 4. Maps show: A) The indentation hardness (H , mean value 0.869 GPa), and B) the plane strain modulus (\bar{E} , mean value 12.62 GPa). Both maps are color coded around the mean value: yellow to red for values higher than the mean, and turquoise to blue for values lower than the mean. Each color represents steps of 0.05 and 0.5 GPa for H and \bar{E} , respectively. Values below the lowest contour level are shown as black. Indentations were performed on two separate grids; indents were set 15 μm apart in each grid. C) Regions of lower-than average hardness; see text for details.

high modulus do not coincide with those of high hardness, and there is no apparent correlation with the variation in jaw texture. The hard, serrated side (top of maps in Figure 5) shows lower-than-average modulus. This combination of high hardness and lower-than-average modulus is consistent with the function of the serrated side of the jaw, that is, to grasp objects by a pincer-like action, which in turn, is consistent with the need for a hard and wear-resistant material.

To test the statistical significance of the spatial distribution of mechanical properties, we divided the jaw cross-section into three regions as indicated in Table 2: the serrated side, the flat side, and the bulgy side. The average values of hardness and reduced modulus in the three regions are given in the table. The mechanical properties of the three areas were compared

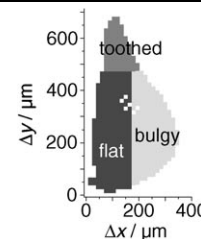
by using a Student's t -test, which showed that the reduced modulus was larger in the bulgy side than in either the serrated or flat sides ($P < 10^{-4}$), whereas the difference in reduced modulus between serrated and flat sides was insignificant ($P = 0.078$). The serrated side is harder than both the flat and bulgy sides, and the bulgy side is in turn harder than the flat one ($P < 10^{-4}$). Jaw hardness is highest on the outer rim of the toothed side of the jaw (Figure 5, top of map). Additionally, there are hard points in several places along the jaw exterior that are suggestive of a hard outer layer. Note that the indentation was performed on a grid with indents spaced 15 μm apart. Therefore, the current experiment does not have sufficient resolution for it to be possible to decide whether a possible thin hard outer rim (possibly with a thickness of the order of 5 μm) extends along the entire jaw surface. EDS data (not presented here) on the toothed tip of the jaw suggest that there might be a thin outer layer with different composition: points along the jaw surface exhibit an Fe content much higher than in the jaw interior. Ca, Ni, and S were also observed. This iron-containing layer was found only on the bulgy side of the jaw. These observations suggest that there is a very thin outer coating on at least part of the jaw, which potentially imbues the jaw surface with extra hardness. Studies

of several other cross-sections showed that iron was concentrated in a thin rim on the toothed and parts of the bulgy side of the jaw (data not shown). The extent of the iron coating varied somewhat and the iron content was below the detection limit of the experiment in some samples. Whether this variability is due to variations in wear, age, growth conditions, or other factors is presently unclear.

By performing mass spectrometric analysis of the hydrolysis products, we found that the jaws contain a large number of amino acids modified by post-translational modification,^[14–16,20] as summarized in Table 1. These included substitutional modifications of His and Tyr as well as cross-linked tyrosines. We found no less than 16 Tyr derivatives, six of which have not previously been observed in nature. Halogenated tyrosines

Table 2. Mechanical properties of various regions of the jaw cross-section as determined by nanoindentation. The three areas are indicated in the sketch on the right. Indents in the channels (white points in the sketch) were excluded. For each area, the mean value, standard deviation from the mean (SD), and standard error of the mean ($\text{SEM} = \text{SD}/n^{1/2}$, where n is the number of observations) are given.

Region	Indents	H [GPa]			\bar{E} [GPa]		
		value	SD	SEM	value	SD	SEM
serrated	86	1.027	0.130	0.014	12.38	1.26	0.14
flat	282	0.792	0.113	0.007	12.07	1.90	0.11
bulgy	242	0.903	0.167	0.011	13.34	1.47	0.09



and cross-linked tyrosines are well known in invertebrate scleroproteins,^[15,19,20] as is dihydroxyphenylalanine (DOPA), which additionally is a capable metal chelator and is widespread in invertebrate mechanical tissues.^[21] Two new modifications of His were found, dibromo- and bromiodohistidine. Diiodohistidine was also found in the *Nereis* jaw; it is otherwise known from thyroglobulin in man and rat^[22] and, interestingly in the present context, black coral (*Antipatharia*) skeletons.^[23–25]

The presence of DOPA, dityrosines, and halogenated Tyr and His in the jaws is suggestive of phenolase and/or haloperoxidase action. DOPA can be obtained from phenolase (also called tyrosinase or catechol oxidase) activity.^[21,26] Peroxidase uses H₂O₂ to catalyze a one-electron oxidation of Tyr to form a tyrosine free radical.^[27] Tyrosine free radicals can combine with one another, hydroxyl radicals, and halogens to form dityrosine, DOPA, and halogenated Tyr, respectively. Halogenation can also occur through the action of haloperoxidases, which oxidize the halogens prior to reaction with the organic substrate.^[28] In the jaws of the related worm *Glycera convoluta*, peroxidase activity has been established histochemically.^[29] Furthermore, phenolase and peroxidase activity has been detected in the setae of *Syllis cornut*.^[30] These observations show that both types of enzymes are present in polychaetes. The noncolocalization of I and Br in the *Nereis* jaw (Figure 3E) suggests that Tyr halogenation might be carried out by distinct and differentially distributed haloperoxidases.

Fletcher used radiolabeled iodide to show that *Nereis diversicolor* accumulates iodine from the environment, which leads to whole body concentrations 5000 times that of the environment.^[31] Over about 30 h, the iodide was partly redistributed from the coelom to the hard tissues including the jaws. Some of the iodine remained as iodide while the rest was distributed over various forms, one of which was shown to be iodotyrosine. The fact that iodine is taken up and concentrated from the environment, subsequently moved to the hard tissues, and there bound to tyrosine, strongly suggests that *Nereis* has a specific mechanism to regulate and process iodine. Our observation of a multitude of post-translational modifications in the jaws suggests that the setae of *Nereis* should be another rich source of modified amino acids. The setae of *Petta pusilla* exhibit a gradient of bromine and iodine that increases from the base to the tip.^[32] The two halogens are found in higher concentration towards the surface of the setae, which according to histochemical analysis also contain Tyr, especially towards the surface. This strongly suggests that similar halogenation reactions take place in that case as well. The amino acids are not distributed evenly in the jaw of *Nereis virens*. The concentration of His, like Zn and Cl, is already known to be highest near the jaw tip.^[10] We now find that while the His concentration increases towards the tip, that of Gly, Asp/Asn, and Tyr are almost constant (Figure 6). In direct opposition to His, the concentration of the hydrophobic Ala decreases from jaw base to tip. In this connection, it is worth stressing that the jaws of the *Perinereis cultrifera*, another nereid polychaete worm, have an amino-acid composition quite similar to that of *N. virens*,^[33] notably a large Gly content and significant amounts of Asp/Asn, Glu/Gln, His, Tyr, and Ala. The His content reported for *P. cultri-*

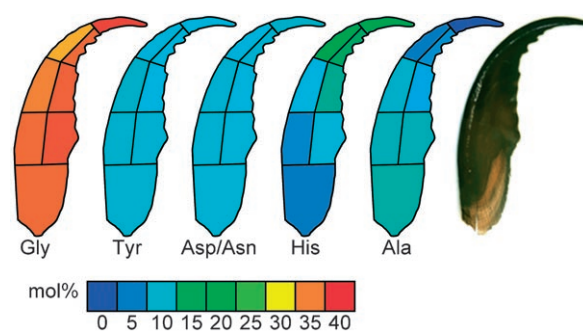


Figure 6. Spatial variations of amino-acid composition in the jaws. The increase in His content towards the tip^[10] is accompanied by a corresponding decrease in Ala concentration. The Gly, Tyr, and Asp/Asn concentrations show only small variations.

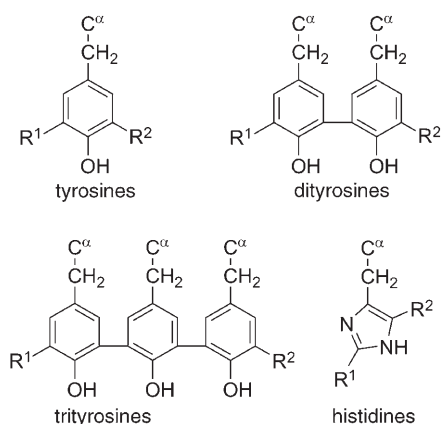
fera is, however, smaller (8% rather than 19%) and the Ala content is higher (assuming that there was complete hydrolysis). Also, the zinc content in *P. cultrifera* jaws is lower than that in *N. virens*.^[7] The large Tyr content found in both animals (8%) suggests that amino acid cross-linking occurs in *P. cultrifera* as well.

Iodinated His has been found in the skeleton of black corals (*Antipatharia*),^[23] which contains large quantities of iodine (estimates vary, but recent values are around 2–5% by weight^[24,25]). Antipatharian skeletons are not mineralized. They contain 10–15 wt% chitin,^[25] but are otherwise proteinaceous.^[23–25] The protein part of the skeletons contains on the order of 15% His and 2% monoiodohistidine in the two species that have been studied.^[23] Interestingly, there are only very small quantities of transition metals in the antipatharian skeletons,^[25] which implies that His does not function as a metal chelator in this case. The skeletons also contain Tyr in quantities (~9%) that are similar to those found in *Nereis* jaws, which is consistent with protein cross-linking. The skeletons differ from *Nereis* jaws in that they are poorer in acidic amino acids and in Gly (about 32% Gly compared to 37.7% in *Nereis* jaws) but richer in hydrophobic amino acids—Ala, Val, Ile, Leu, and Phe make up around 20% of the protein in the antipatharian skeleton compared to only 8.5% in *Nereis* jaws. By using cross-polarization magic-angle-spinning (CPMAS) solid-state ¹³C and ¹⁵N NMR it has been shown that the ring nitrogen atoms of His can be involved in cross-linking with catecholamines, which are in turn linked to chitin by the catechol functionality, in the cuticle of the tobacco hornworm *Manduca sexta*.^[34,35] Tandem mass spectrometry (MS–MS) analyses have confirmed that catechol–His cross-links are present in the *M. sexta* cuticle but that they result from covalent-bond formation between His and DOPET (2-(3,4-dihydroxyphenyl)ethanol) rather than dopamine.^[36] Based on these observations we tentatively suggest that His might be involved in protein cross-linking in *Nereis* jaws as previously proposed by Holl et al. for the antipatharian skeleton.^[37] In our present work, we have not obtained proof for such cross-links, which suggests that they do not dominate in *Nereis* jaws. Future work is, however, likely to reveal additional post-translational modifications as we were not able to positively identify the chemical structure of all promising HPLC

fractions. These considerations indicate that *Nereis* jaws will likely continue to provide valuable insights into protein cross-linking in the future.

Conclusion

The variations in modulus and hardness do not appear to be correlated with the distribution of bromine and iodine, and thus the influence of these heavy halogens on mechanical properties remains unclear. The presence of halogenated di- and trityrosines suggests that protein cross-linking occurs in the jaw. Given the localization of Br and I towards the outer



Scheme 1. Side chains of post-translationally modified amino acids found in *Nereis* jaws.

surface, the jaw appears to be encased by a halogenated cross-linked protein. This casing could play several roles. First, the combination of cross-linking with halogen bonding^[38] should stabilize the jaw and render it insoluble and less susceptible to chemical and enzymatic attack.^[19,39] The casing can also serve as a straightjacket for the fibrous zinc-binding proteins in the core. Indeed, we have not been able to extract protein from whole jaws, but have succeeded in obtaining soluble proteins from crushed jaws that have their interior exposed.^[40] Secondly, this outer casing could also play a mechanical role—possibly in combination with an additional metal-containing coating—as an abrasion/wear-resistant layer, though our present results indicate that such a feature has a smaller effect than other, structural variations. A recent report that *Nereis* burrows through the sediment by using its everted pharynx for crack propagation^[41] is particularly interesting and suggests that the jaws might also have an important nonpredatory role. The jaws, which sit at the pharynx tip, are exposed during eversion; this suggests that they could be mechanically adapted to this behavior as well.

Experimental Section

Specimens: *N. virens* specimens were obtained live from the Maine Bait Company (New Castle, Maine, USA). Upon arrival, they were killed by rapid freezing at -80°C . Jaws were dissected from freshly

thawed animals, washed three times with guanidine-HCl (2.4 M)/acetic acid (5%) and with distilled water (5 \times), and then air-dried.

Nanoindentation: For nanoindentation, jaws were embedded in EpoFix (Electron Microscopy Sciences, Hatfield, PA, USA). The desired cut was made by using a Leica ultramicrotome and a Diatome diamond knife (Electron Microscopy Sciences). Nanoindentation measurements were performed by using a Hysitron TriboIndenter (Hysitron, Minneapolis, MN, USA). The indenter was a cube corner diamond-indenter tip with a curvature radius of 40–60 nm (Hysitron). The following indentation program, which was the result of several test measurements, was used: load to 500 μN at 100 $\mu\text{N s}^{-1}$, hold for 60 s, unload at 100 $\mu\text{N s}^{-1}$. The 60 s hold period was found to be sufficient for relaxation of viscoelastic effects. The indentation data were measured on two grids each with 15 μm spacing between indents, which generated a total of 1032 indents. Among these, 610 were located within the test specimen whereas the others were located either in the surrounding epoxy or within the channels described below. The indentation hardness (H) and plane strain modulus (\bar{E}) were determined by using the method of Oliver and Pharr.^[42] (The latter quantity is related to Young's modulus E through:

$$\bar{E} = \frac{E}{1-\nu^2}$$

where ν is Poisson's ratio. For all realistic estimates of ν , \bar{E} is about 10% greater than E and is insensitive to the selection of ν .) The trends observed herein are in accord with preliminary data on a different section on the same jaw.^[43]

Microscopy and elemental mapping: The jaw section investigated by nanoindentation was further studied by environmental scanning electron microscopy (ESEM) by using a FEI XL30 with a field emission gun. Other sections, prepared in the same way, were also examined in the ESEM. The samples were uncoated and the microscope was operated in environmental mode. Images were made with both BSE detection, in which contrast is roughly proportional to the local electron density, and a large field detector for backscatter electron imaging. X-ray microanalysis and elemental mapping were performed by using a Princeton gamma tech PRISM IG energy-dispersive spectrometer.

Amino acid analysis: *Nereis* jaws, or portions thereof, were hydrolyzed in vacuo in HCl (6 N) with phenol (5%; antioxidant) at 110°C . Although the duration of standard protein hydrolysis is routinely 24 h, we also performed 48 and 72 h hydrolyses for comparison. In the case of *Nereis* jaws, the 24 h protein hydrolysis proved to be incomplete, as judged by the variability of the amino-acid composition. After 48 and 72 h, however, amino-acid compositions for the jaw sections became reproducible. Thus, 48 h was selected as the standard hydrolysis time. Following hydrolysis, the acid was removed by flash evaporation at 60°C under vacuum and the dried residue was resuspended in NaS (Beckman-Coulter) and applied to a Beckman 6300 Autoanalyzer by using an extended elution program,^[44] and a sodium high performance column (Beckman-Coulter). Signal analysis and integration was carried out by using a ChemStation (Agilent, Wilmington, DE, USA).

Post-translationally modified amino acids: Post-translationally modified amino acids were isolated by using the following protocol: jaws (28.5 mg) were hydrolyzed in vacuo for 48 h in HCl (6 N, 8 mL; Sigma) and saturated phenol (30 μL ; Pierce) at 110°C . The brown hydrolysate was fractionated by gel-filtration chromatography on a 90×1.5 cm Bio-Gel P2 column, and eluted with acetic acid (2%) at 19.2 mL h^{-1} . UV spectra of the individual fractions

were measured with a Milton Roy Spectronic 501&601 spectrophotometer and fractions that absorbed at $\lambda = 280$ nm were pooled, as shown in Figure S1 (see Supporting Information). The pooled fractions were further fractionated by HPLC by using a C-18 column (Perkin-Elmer, part no. 0712-0073) with an acetonitrile/TFA (0.1%; trifluoroacetic acid) versus H₂O/TFA (0.1%). The elution program was: 0% acetonitrile (ACN) from 0–10 min, 10% ACN from 10–40 min, 20% ACN from 40–50 min, a gradient 20–100% ACN from 50–65 min, and from 100–0% ACN from 65–70 min. One of the P2 column peaks (peak 3; see Supplementary Information Figure S1) was not separated sufficiently by the first elution program, and a second program was developed by using the same solvent system: 0% ACN from 0–10 min, gradient 0–10% ACN from 10–15 min, gradient 10–20% ACN from 15–50 min, gradient 20–40% ACN from 50–60 min, gradient 40–100% ACN from 60–65 min, and gradient 100–0% ACN from 65–70 min.

Promising HPLC fractions (judged by their absorbance at $\lambda = 280$ and 215 nm) were selected for structure elucidation using mass spectrometry. Positive ion TOF-ESIMS was performed on a PE Sciex QStar quadrupole/time-of-flight tandem mass spectrometer. Typical settings were a capillary voltage of 3.5 kV, cone tension of 45 V, and collision voltage of 10 V for MS. Some candidate structures were further analyzed by MS-MS on the same instrument when the MS spectrum was not deemed adequate for direct identification. The collision voltage was varied for each target amino acid so that reasonable decomposition patterns that allowed positive identification of the amino acid could be obtained (see Supporting Information). We also performed analyses on a couple of standard amino acids, which included tyrosine, 3,5-dibromotyrosine, O-methyl-DOPA, and 3-monoiodotyrosine (Sigma), by using similar settings with the same instruments. They showed spectra analogous to those from the jaws. The MS-MS spectrum of dityrosine was compared to the literature spectrum^[45] and found to match completely.

Acknowledgements

We thank Dr. Jose Saleta of the Micro-Environmental Imaging & Analysis Facility of the Donald Bren School of Environmental Science & Management, UCSB for kind assistance with the ESEM measurements, and Dr. James Pavlovich for his assistance with the mass spectrometric measurements. We thank the participants of the Thursday NASA URETI meetings, in particular members of the Waite, Stucky, Morse, and Hansma groups for helpful discussions. Financial support from NIH BRP DE014672, additional funding from the Fonds zur Förderung der Wissenschaftlichen Forschung (Austria) Awards J2184 and T190 (H.C.L.), and the Danish Natural Sciences Research Council (H.B.) is gratefully acknowledged. H.B. further thanks the Danish Natural Sciences Research Council and the Danish Technical Research Council for a Steno research-assistant professor fellowship, which funded the final stages of this project. This research was partially supported by University of California Systemwide Biotechnology Research & Education Program GREAT Training Grant 2005-240. This work made use of MRL Central Facilities supported by the MRSEC Program of the National Science Foundation under award No. DMR00-80034.

Keywords: amino acids • bioinorganic chemistry • halogenation • post-translational modifications • proteins

- [1] S. Mann, *Bioinorganic Chemistry: Principles and Concepts in Bioinorganic Materials Chemistry*, Oxford University Press, Oxford, **2001**.
- [2] H. A. Lowenstam, *Science* **1962**, *137*, 279.
- [3] H. A. Lowenstam, *Science* **1967**, *156*, 1373.
- [4] A. Warén, S. Bengtson, S. K. Goffredi, C. L. Van Dover, *Science* **2003**, *302*, 1007.
- [5] H. C. Lichtenegger, T. Schöberl, M. H. Bartl, H. Waite, G. D. Stucky, *Science* **2002**, *298*, 389.
- [6] H. C. Lichtenegger, H. Birkedal, D. M. Casa, J. O. Cross, S. M. Heald, J. H. Waite, G. D. Stucky, *Chem. Mater.* **2005**, *17*, 2927.
- [7] G. W. Bryan, P. E. Gibbs, *J. Mar. Biol. Assoc. UK* **1979**, *59*, 969.
- [8] G. W. Bryan, P. E. Gibbs, *J. Mar. Biol. Assoc. UK* **1980**, *60*, 641.
- [9] M. Eriksson, M. Elfman, *Lethaia* **2000**, *33*, 75.
- [10] H. C. Lichtenegger, T. Schöberl, J. T. Ruokolainen, J. O. Cross, S. M. Heald, H. Birkedal, J. H. Waite, G. D. Stucky, *Proc. Natl. Acad. Sci. USA* **2003**, *100*, 9144.
- [11] J. G. McClements, S. A. Smith, P. Wyeth in *The Chemistry of the Copper and Zinc Triads* (Eds.: A. J. Welch, S. K. Chapman), The Royal Society of Chemistry, Cambridge, UK, **1993**, p. 58.
- [12] J. H. Waite, H. C. Lichtenegger, G. D. Stucky, P. Hansma, *Biochemistry* **2004**, *43*, 7653.
- [13] S. Suresh, *Science* **2001**, *292*, 2447.
- [14] R. Amadò, R. Aeschbach, H. Neukom, *Methods Enzymol.* **1984**, *107*, 377.
- [15] S. Hunt, *Methods Enzymol.* **1984**, *107*, 413.
- [16] R. G. Krishna, F. Wold in *Advances in Enzymology and Related Areas of Molecular Biology*, Vol. 67 (Ed.: A. Meister), Wiley, New York, **1993**, p. 265.
- [17] P. J. W. Olive in *Skeletal Growth of Aquatic Organisms: Biological Records of Environmental Change*, Vol. 1 (Eds.: D. C. Rhoads, R. A. Lutz), Plenum, New York, **1980**, p. 561.
- [18] J. Goldstein, J. Newbury, D. Joy, C. Lyman, P. Echlin, E. Lifshin, L. Sawyer, J. Michael, *Scanning Electron Microscopy and X-ray Microanalysis*, 3rd ed., Kluwer Academic/Plenum, New York, **2003**.
- [19] C. Broomell, M. A. Mattoni, F. W. Zok, J. H. Waite, *J. Exp. Biol.* **2006**, in press.
- [20] J. H. Waite, M. L. Tanzer in *CRC Handbook of Biochemistry in Aging* (Ed.: J. R. Florini), CRC Press, Boca Raton, **1981**, p. 195.
- [21] J. H. Waite, *Comp. Biochem. Physiol. Part B* **1990**, *97*, 19.
- [22] J. C. Savoie, P. Thomopoulos, F. Savoie, *J. Clin. Invest.* **1973**, *52*, 106.
- [23] W. M. Goldberg, *Mar. Biol.* **1976**, *35*, 253.
- [24] W. M. Goldberg, *Mar. Biol.* **1978**, *49*, 203.
- [25] W. M. Goldberg, T. L. Hopkins, S. M. Holl, K. Schaefer, K. J. Kramer, T. D. Morgan, K. Kim, *Comp. Biochem. Physiol.* **1994**, *107B*, 633.
- [26] C. Gerdemann, C. Eicken, B. Krebs, *Acc. Chem. Res.* **2002**, *35*, 183.
- [27] H. Eickhoff, G. Jung, A. Rieker, *Tetrahedron* **2001**, *57*, 353.
- [28] A. Butler, J. V. Walker, *Chem. Rev.* **1993**, *93*, 1937.
- [29] C. Michel, M.-T. Fonce-Vignaux, M.-F. Voss-Foucart, *Bull. Biol. Fr. Belg.* **1973**, *107*, 301.
- [30] C. Michel, J. Vovelle, *Bull. Soc. Zool. Fr.* **1974**, *99*, 175.
- [31] C. R. Fletcher, *Comp. Biochem. Physiol.* **1970**, *35*, 105.
- [32] J. Vovelle, M. Grassat, M. Truchet, *Cah. Biol. Mar.* **1983**, *24*, 309.
- [33] M.-F. Voss-Foucart, M.-T. Fonce-Vignaux, C. Jeuniaux, *Biochem. Syst.* **1973**, *1*, 119.
- [34] J. Schaefer, K. J. Kramer, J. R. Garbow, G. S. Jacob, E. O. Stejskal, T. L. Hopkins, R. D. Speirs, *Science* **1987**, *235*, 1200.
- [35] A. M. Christensen, J. Schaefer, K. J. Kramer, T. D. Morgan, T. L. Hopkins, *J. Am. Chem. Soc.* **1991**, *113*, 6799.
- [36] J. L. Kerwin, F. Turecek, R. Xu, K. J. Kramer, T. L. Hopkins, C. L. Gatlin, J. R. Yates III, *Anal. Biochem.* **1999**, *268*, 229.
- [37] S. M. Holl, J. Schaefer, W. M. Goldberg, K. J. Kramer, T. D. Morgan, T. L. Hopkins, *Arch. Biochem. Biophys.* **1992**, *292*, 107.
- [38] P. Auffinger, F. A. Hays, E. Westhof, P. S. Ho, *Proc. Natl. Acad. Sci. USA* **2004**, *101*, 16789.
- [39] S. C. B. Myneni, *Science* **2002**, *295*, 1039.
- [40] C. Broomell, R. K. Khan, J. H. Waite, **2005**, unpublished results.
- [41] K. M. Dorgan, P. A. Jumars, B. Johnson, B. P. Boudreau, E. Landis, *Nature* **2005**, *433*, 475.

[42] W. C. Oliver, G. M. Pharr, *J. Mater. Res.* **1992**, *7*, 1564.

[43] H. Birkedal, C. Broomell, R. K. Khan, N. Slack, H. C. Lichtenegger, F. Zok, G. D. Stucky, J. H. Waite, *Mater. Res. Soc. Symp. Proc.* **2005**, *873*, L2.8.1.

[44] J. H. Waite, *Anal. Biochem.* **1991**, *192*, 429.

[45] F. Hanft, P. Koehler, *J. Agric. Food Chem.* **2005**, *53*, 2418.

Received: April 18, 2006

Published online on August 9, 2006
